Plant Physiology Preview. Published on October 21, 2019, as DOI:10.1104/pp.19.00728

A deep learning-based approach for high-throughput hypocotyl phenotyping

Orsolya Dobos[1,2], Peter Horvath[3], Ferenc Nagy[1], Tivadar Danka[3*], András Viczián[1*]

Author affiliations:

1. Institute of Plant Biology, Biological Research Centre of the Hungarian Academy of Sciences, Temesvári krt. 62, H-6726 Szeged, Hungary
2. Doctoral School in Biology, Faculty of Science and Informatics, University of Szeged, Szeged, H-6726, Hungary.
3. Institute of Biochemistry, Biological Research Centre of the Hungarian Academy of Sciences, Temesvári krt. 62, H-6726 Szeged, Hungary

Short title:

Deep learning for high-throughput phenotyping

One-sentence summary:

A deep learning-based algorithm provides an adaptable tool for determining hypocotyl or coleoptile length of different plant species.

Keywords:

plant phenotyping, Arabidopsis, computer vision, machine learning, deep learning

Author contributions:

O.D., T.D., P.H., F.N. and A.V. conceived the original research plans; O.D. performed the experiments; A.V. supervised the experiments, T.D. developed the algorithm; F.N. commented on the manuscript, O.D., T.D. and A.V. analysed the data and wrote the article with contributions of all the authors.

Funding Information:

O.D., A.V. and F.N. were supported by grants from the Economic Development and Innovation Operative Program (GINOP-2.3.2-15-2016-00001 and GINOP-2.3.2-15-2016-00015) and from the Hungarian Scientific Research Fund (OTKA, K-132633).
T.D. and P.H. acknowledge support from the HAS-LENDULET-BIOMAG and from the European Union and the European Regional Development Fund GINOP-2.3.2-15-2016-00026.

*Authors for Contact:

Tivadar Danka: tdanka@brc.hu
András Viczián: aviczian@brc.hu

Abstract

Hypocotyl length determination is a widely used method to phenotype young seedlings. The measurement itself has advanced from using rulers and millimetre papers to assessing digitized images but remains a labour-intensive, monotonous and time-consuming procedure. To make high-throughput plant phenotyping possible, we developed a deep learning-based approach to simplify and accelerate this method. Our pipeline does not require a specialized imaging system but works well with low-quality images produced with a simple flatbed scanner or a smartphone camera. Moreover, it is easily adaptable for a diverse range of datasets not restricted to Arabidopsis (*Arabidopsis thaliana*). Furthermore, we show that the accuracy of the method reaches human performance. We not only provide the full code at https://github.com/biomag-lab/hypocotyl-UNet, but also give detailed instructions on how the algorithm can be trained with custom data, tailoring it for the requirements and imaging setup of the user.

Introduction

Monitoring different aspects of seedling development requires determining certain physical dimensions of the plantlet. Among these, measurement of hypocotyl length is a key phenotypic trait to monitor and quantify different responses. Hypocotyl cells are formed in the embryo and their eventual number set after only a few cell divisions. During seedling growth, the length of the hypocotyl is determined by no further cell divisions but by the elongation of hypocotyl cells (Gendreau et al., 1997). Hypocotyl growth is regulated by a complex network of external and internal factors. Different hormones (auxins, ethylene, cytokinins, abscisic acid, gibberellins and brassinosteroids) are involved in the response (Vandenbussche et al., 2005; Hayashi et al., 2014). Among external cues, gravity not only determines the direction of growth (away from the soil surface) but also affects the hypocotyl elongation (Soga et al., 2018). Our knowledge about how light regulates hypocotyl elongation is much more detailed. Without light, etiolated plants develop elongated hypocotyls, whereas light triggers photomorphogenic development with characteristic, fluence rate-dependent inhibition of hypocotyl elongation, which is one of the key features of the so-called photomorphogenic growth (Fankhauser and Casal, 2004; Arsovski et al., 2012). The role of different light-sensing molecules (photoreceptors) has been revealed in this response: phytochrome B (phyB) is the dominant photoreceptor in red (R), phyA in far-red (FR) and cryptochrome 1 and 2 in blue (B) light (Lin et al., 1996; Nagy and Schäfer, 2002). Photomorphogenic ultraviolet B (UV-B) radiation also induces inhibition of hypocotyl elongation (Kim et al., 1998) involving pathways controlled by UV RESISTANCE 8 (UVR8) UV-B receptor (Favory et al., 2009). Fluence rate response curves are used to depict hypocotyl length change over broad light fluences, demonstrating the involvement of specific receptors and their signalling partners in the examined responses. Temperature is the third external cue affecting hypocotyl length. It was recently shown how lower temperature shortens hypocotyl length via phyB in light (Jung et al., 2016; Legris et al., 2016; Casal and Qüesta, 2018).

These examples show that hypocotyl length is a seedling phenotypic trait of particular importance. On one hand it indicates the functionality of the examined signalling pathway(s), and on the other hand it is relatively easy to measure, generating quantified data of the observed response. Thus researchers measure hypocotyl length (i) to compare the effect of different light, hormone, etc. treatments, (ii) to analyse the role of signalling components

using mutants and overexpressor lines and (iii) to perform different reverse and forward genetic (screening) approaches.
The methodology of the hypocotyl measurement has changed over time. In early studies hypocotyls were simply measured by hand one-by-one using a ruler or millimetre paper, in many cases rounding the observed value to the nearest millimetre (Köhler, 1978; Liscum and Hangarter, 1991; Pepper et al., 2001; Dieterle et al., 2005). A more precise and most widely applied quantification procedure involves the arrangement of seedlings on sticky surfaces or agar plates, subsequent scanning or photographing and measurement of hypocotyl length using a digital image processing software (Young et al., 1992; Borevitz and Neff, 2008; Ádám et al., 2013; Das et al., 2016). This approach gives the opportunity to store hypocotyl images and measure them at a later time while involving other experimenters in the measurement procedure. To speed up this process and reduce the invested work-time, different applications have been created to automate the quantification of hypocotyl length (Sangster et al., 2008; Wang et al., 2009; Cole et al., 2011; Spalding and Miller, 2013). These image processing tools have the potential to replace error prone and labour intensive manual image processing and to advance plant phenotyping by enabling high-throughput data analysis. A cornerstone of these algorithms is the plant segmentation, that is, the separation of the plant from the background. This is a difficult task due to the diversity of images, which can be caused, for example, by different image acquisition setups and conditions. However, good segmentation is key to downstream analyses, such as object boundary detection and midline tracking (Spalding and Miller, 2013). In addition to overall plant segmentation, fully automated identification of different plant subparts, such as cotyledons, roots and seedcoats, is a significant challenge, which has not been solved reassuringly in the previous efforts. For hypocotyl length measurement, a major difficulty is the localization of hypocotyl-root junction and robust identification of the cotyledons. Tools based on classical segmentation algorithms have troubles identifying these parts for several reasons, including high variance in phenotypes, variable imaging conditions or noisy images. Since imaging methods are very different from lab to lab and no gold standard is available, it is essential to provide a data analysis pipeline which works robustly for a diverse set of images.

Up until the recent introduction of deep convolutional neural networks (CNN), a robust image analysis pipeline was extremely difficult to achieve. In contrast to classical methods, modern deep convolutional networks can surpass human performance in many image processing tasks, including object classification and detection (Geirhos et al., 2018). Instead of relying on hand crafted filters and features, a neural network learns the optimal representation of the data. This makes its performance exceptionally good, and given enough data, a well-trained neural network can generalize for a wide range of datasets. For plant phenotyping, these developments have yielded advances in trait identification and genotype/phenotype classification (Pound et al., 2017; Namin et al., 2018).

In this paper, we present a deep learning-based approach which is able to provide quantified seedling phenotype data in a high-throughput manner. Compared to earlier tools, ours is fully-automated and achieves human expert accuracy on length measurement tasks for various plant species, such as Arabidopsis (*Arabidopsis thaliana*), mustard (*Sinapis alba*) and stiff brome (*Brachypodium distachyon*). The method does not require expensive imaging setups, and accurate results can be obtained with a simple flatbed scanner or a smartphone camera. In addition, the measurement itself requires only a few seconds per image, thus reducing the time spent by several orders of magnitude. We provide full access to our algorithm as it is open source and also give detailed instructions how to perform training for customised hypocotyl length determination approaches.

Results

The architecture of the algorithm

To extract the length data from images, first we perform segmentation, followed by the skeletonization of the segmented objects to be measured (Fig. 1A). In the case of a typical seedling, each image is segmented into three non-overlapping parts: 1) background 2) hypocotyl 3) non-hypocotyl seedling area. (The latter category differs between species, thus different non-hypocotyl parts should be defined accordingly.) Central to our approach is the U-Net deep CNN for segmentation, which is particularly excellent for finding thin objects. It has been applied on various problems with success, such as detecting cell nuclei in microscopic images or identifying subparts of the brain on MRI scans (Ronneberger et al., 2015; Buda et al., 2019). U-Net is able to identify specific parts of the plants in images and separate them from the background. On a provided image, U-Net applies convolution operations with various filters followed by maximum pooling repeatedly, producing the segmentation masks. The major difference, as opposed to classical image processing algorithms, is that the filters used by the network are not given in advance but learned from the data during the so-called training phase. In this phase, the segmentation masks provided by the expert are shown for the algorithm several times, which is then able to learn how to classify each pixel either as background or as a specific plant organ. This training process gives rise to filters which are best suited for the task and data, resulting in an extremely robust and adaptable method.

After the specific plant parts are segmented and identified, the binary images of all identified hypocotyls are skeletonized (Lee et al., 1994). Skeletonization is the reduction of binary shapes to 1 pixel-wide representations, a curve in the case of hypocotyls. This operation allows the length measurement of spatial objects. On the skeleton image, components representing hypocotyls were measured by calculating the number of pixels for each identified object and then converted from pixel unit to *mm*. Pixel to *mm* calculations were performed by either scaling directly with the DPI (dots-per-inch) value of the image or using a reference object on each image. After the measurement, very small objects, which are most likely due to segmentation errors, are filtered out. Finally, the obtained results are exported as an RGB image (Fig. 1B) and a *csv* file, ready for downstream analysis.

The choice of the convolutional network architecture

In general, a CNN repeatedly performs convolutional, pooling and in some instances, batch normalizing operations, eventually extracting a feature-level representation of the image. This is called encoding. During this part, information is compressed and can be lost during the pooling steps. For tasks such as image classification, this is not a problem (Pound et al., 2017). However, for semantic segmentation tasks, the network is required to reconstruct the pixel-level segmentation mask, which is achieved by upsampling the feature-level representation. In this decoding step, the information lost during encoding cannot be recovered and will result in suboptimal results for small or thin objects, such as hypocotyls in our case. This problem was solved with the introduction of U-Net (Ronneberger et al., 2015), originally created to find cells in microscopic images where the cells can grow on each other, having only a thin (occasionally 1-2 pixel wide) region separating them. This is achieved by storing the intermediate feature-level representations before each pooling in the encoding step, then feeding this data to the corresponding upsampling layer. Ever since its inception, U-Net has become a state-of-the-art architecture for semantic segmentation. Because of its performance on small or thin objects, this choice of architecture was ideal for our purposes. To add a regularizing term and accelerate training speed, we have added batch normalizing layers after convolutional blocks (Ioffe and Szegedy, 2015).

Phenotypic analysis of Arabidopsis seedlings

Determining hypocotyl length of Arabidopsis seedlings is a key phenotyping procedure in myriads of studies; thus it was obvious to test our algorithm on this model plant first. We simply grew seedlings on wet filter papers under different fluences of monochromatic light sources, laid them on agar plates, scanned them and then used these images to train the algorithm. Altogether we annotated about 2500 hypocotyls and corresponding non-hypocotyl plant parts during this procedure. To test the trained algorithm, we grew seedlings under different fluences of monochromatic R light as a routine treatment for phytochrome studies. Fig. 2A and Supplemental Fig. S1 show how the algorithm recognized long and short hypocotyls belonging to those plants which grow under low or high fluences of light, respectively. The fluence rate graph plotting of the measured hypocotyl length values demonstrates that the algorithm determined values similar to the human experimenters (Fig. 2B). To further test the versatility of the algorithm we analysed hypocotyls of seedlings grown in FR and B light when the inhibition of hypocotyl elongation is mediated by phyA and cryptochrome photoreceptors, respectively. Additionally we analysed etiolated seedlings grown in darkness, which are used as important controls in photobiological studies. We found the performance of the algorithm is comparable to humans under these conditions, and the measurement works well even with pale, almost colourless etiolated seedlings (Supplemental Fig. S2, Fig S3, Fig. S4, Fig S5). It was tempting to further examine seedlings which have completely different body architecture. For this purpose, we grew plantlets on plant medium containing sugar with white light illumination. These seedlings have thick hypocotyls, fully developed and opened green cotyledons and long roots. Our results show that the algorithm is capable of measuring the hypocotyls of seedlings grown under light/dark cycles or under continuous white light supplemented with or without photomorphogenic (non-damaging) UV-B irradiation (Supplemental Fig. S6 and Fig. S7).

Application of the algorithm on different plant species

To test the usability of our algorithm on other species besides Arabidopsis, we chose mustard (*Sinapis alba)*. *Sinapis alba* was an experimental object widely used a few decades ago to examine the dependency of hypocotyl elongation on different irradiation protocols. These works revealed the basic mechanisms of phytochrome action many years before identifying the involved molecular pathways or even the genes coding the photoreceptors (Schopfer and Oelze-Karow, 1971; Wildermann et al., 1978a; Wildermann et al., 1978b). A recent study demonstrates that determining the hypocotyl elongation of *Sinapis alba* seedlings as a phenotypic marker is still in use to monitor hormonal changes under different irradiation conditions (Procko et al., 2014).

The *Sinapis alba* plantlets were grown on agar plates under constant white light for 4 days. These seedlings were too bulky to scan them with a flatbed scanner like we did with Arabidopsis seedlings. For this reason, images were taken with a smartphone. We used these images to train our algorithm to identify pixels belonging to *Sinapis alba* hypocotyls

and to determine hypocotyl length. During the training phase we annotated about 250 hypocotyls and corresponding non-hypocotyl plant parts before performing the presented measurement. Fig. 3 and Supplemental Fig. S8 demonstrate that even low numbers of seedlings were sufficient to train the algorithm and determine hypocotyl length with high accuracy, which is comparable to the performance of human experts.
We further tested the versatility of the algorithm by analysing monocotyledonous plants. In monocots, the coleoptile growth is a widely used phenotypic trait instead of the more difficultly observable hypocotyl. We chose stiff brome (*Brachypodium distachyon*), which is a small-sized model plant having a compact and sequenced genome (International Brachypodium Initiative, 2010) and an existing transformation system (Alves et al., 2009). These make it an ideal grass model species with emerging importance (Scholthof et al., 2018). We grew the (*Brachypodium distachyon)* plants under different light fields for 4 days and took photos of them with a smartphone camera. In this case we used 8 images containing about 100 plants to train the algorithm. Fig. 3 and Supplemental Fig. S9 show how the algorithm processed the images and how it measured coleoptile length on the test images. The obtained values do not differ from those measured by the human experts, demonstrating the usability of the algorithm to analyse *Brachypodium distachyon* coleoptiles.

Accuracy of the algorithm

To quantitatively assess the performance of our algorithm, we decided to compare the obtained results to the performance of humans. Each measurement was repeated by two human experimenters. For each seedling identified by the algorithm, we calculated measurement accuracy by matching the seedling to the ground truth data provided by the experts (Fig. 4) and calculating the relative error of the measurement. For matching, we first calculated the bounding boxes for each object identified by the algorithm, which is the smallest box containing the segmented object (Fig. 1B). Then the expert provided ground truth segmentation masks were used to check whether there was an actual object in the same spatial location. To see this, bounding boxes of the ground truth masks were also calculated and their position was matched against the position of the algorithm identified object. If a bounding box with at least 10% overlap was found, we matched the two objects and calculated the relative error of the measurement, defined by $|L - M|/L$, where L is the actual length of the hypocotyl (measured by the experts) and M is the result of the measurement (provided by the algorithm). Since the seedlings were placed apart from each other, the possibility of a false matching was minimal. (The 10% overlap criterion was deliberately chosen to be permissive, since requiring larger overlaps essentially guarantees that the relative error is low, thus biasing the accuracy evaluation and masking flaws.) After matching the plants, the false positive (FP) and true positive (TP) ratios were calculated. For a more detailed view on the detection performance, we also calculated the precision and recall values. Precision is defined by $TP/(TP + FP)$, whereas recall was calculated by $TP/(TP + FN)$, with FN denoting the number of false negatives. We calculated accuracy, recall and precision individually for each plant, compared them to the measurement of each expert, then averaged the values. For all of our metrics, a higher value implies a better result (Fig. 4). To put this in perspective, a high precision means that most identified objects are indeed plants (as opposed to segmentation errors), whereas a high recall means that most plants were indeed detected in the image. In general, there is a tradeoff between recall and precision, which is controlled by the strictness of our criteria to accept a match. A too loose criteria lead to an abundance of false detections, resulting in potentially high recall but very low precision. On the other hand, an excessively strict criteria would result in a high false negative rate, leading to low recall and potentially high precision. Thus, the combination of recall and precision together provides a good description on the performance of the algorithm.

To obtain further data to characterize the hypocotyl measurement, as the method itself, both human experimenters measured each plant once more, having one month between their two measurements. Using these repeated measurements, we calculated the intra-expert accuracy exactly as we outlined above, using the two measurements provided by the same expert (Fig. 5). The inter-expert accuracy was calculated using the first measurement of both experts. The algorithm performs exceptionally well on plants with long hypocotyls but with slightly lower reliability in case of the very short seedlings grown under strong FR or B light. We also noted that (i) the performance of humans is also poorer when analysing these plantlets both in the case of intra- or inter-expert comparisons (Fig. 5) and that (ii) the algorithm only gives significant difference between groups when the expert measurements also show significant difference according to Student t-test (Fig. S10).

Discussion

Usability of the method

Hypocotyl growth is controlled by the interplay of different external and internal cues, many of them with reciprocal effects. It follows that hypocotyl length is used (i) to characterise activity of numerous signalling pathways, including those controlled by light, hormones, temperature and gravity and that (ii) determination of hypocotyl length is a widely used basic seedling phenotyping assay. Here we report the development of a deep learning-based algorithm to simplify this measurement and save valuable time for the experimenter. There have been computer-based tools published earlier, but here we demonstrate the suitability of deep learning for quantitative plant phenotyping. This method is applicable to a diverse set of image-based phenotyping problems, not restricted to hypocotyl measurement. Our method uses the U-Net CNN architecture for segmentation and can identify not only hypocotyls, but also roots and cotyledons with previously unprecedented detail. To demonstrate the power of the algorithm, we have shown how it performs on other dicot or monocot seedlings. The method possesses several advantages: (i) no image preprocessing is needed; (ii) the algorithm can handle low quality images, i.e. ones made with a simple smartphone camera; (iii) the algorithm works with different imaging conditions; and (iv) its performance matches human accuracy. Moreover, the whole measurement pipeline is semi-automated, and hypocotyl detection and measurement do not require manual intervention at all. This decreases the execution time with several orders of magnitude: while the expert spends 45 minutes on average manually measuring a complete image containing 270 seedlings having different hypocotyl length and recording the data, our method performs the same task under a minute. With this speedup, high-throughput assays (testing numerous lines, phenotype-based screenings, etc.) are enabled for a wide array of questions.

Assessing our results

To assess the performance of our algorithm, first we focused on Arabidopsis, being the most widely used model plant. Our algorithm performed quite well on seedlings with various body architectures. We tested it on seedlings having short or long, thick or thin hypocotyls; opened or unopened cotyledons with different thickness, size and colour; roots with different length, shape and thickness (Fig. 2 and Supplemental Fig. S1-S7). The accuracy, the

precision and recall values, compared to the results of a human experimenter indicate that the algorithm is suitable to replace manual measurements for a wide array of scenarios (Fig. 4 and Fig. 5). Our data also show that under specific circumstances, when the plants are short (under strong FR and B light), the accuracy of the algorithm is slightly lower compared to human experimenters. The reasons are quite diverse.
(i) The accuracy value is heavily affected by the absolute size of the plant. For example, a 5 pixel error on a 100-pixel-long plant has 0.95 accuracy, whereas on a 20-pixel-sized one, the same absolute error yields 0.75 accuracy. (In our images, a typical hypocotyl length of a seedling grown under high light intensities appeared as only approximately 20 pixels.)
(ii) In case of short and thick hypocotyls, human experts cannot position their region of interest (ROI) at the middle of the hypocotyl. In this case skeletonization can be different from the human ROI placement.
(iii) Misplaced seedlings (hypocotyls touching each other, roots laying over the hypocotyl, etc) or image problems (reflecting plastic plate edges, scratches of the agar surface) disturb the segmentation process but to a lesser extent as with the human experts. These issues can be corrected manually on the generated data, and also a certain carefulness is required during seeding placement onto the agar before the scanning. Another potential source of inaccuracy is the skeletonization of the segmented hypocotyls. Especially for more complicated shapes and cusps, the skeletons may have small additional branches or may not be simply connected at all, which can distort the length measurements.
(iv) Especially in the case of seedlings having short and thick hypocotyls, it is not obvious how to define the border between the hypocotyl and the root. For that, images with higher magnification (i.e. microscopy) should be obtained(Fahn, 1990), which is not manageable when working with a high number of seedlings. This problem is a general caveat of the method: the observable morphological traits at the resolution of the scanned images are not sufficient sometimes to mark precisely where the hypocotyl ends and the root begins.
Taken together, the inaccuracy generated in these ways is an inevitable component of hypocotyl measurement leading to the errors, not only in case of the algorithm, but also in case of measurements made by humans (Fig. 4 and Fig. 5). Similarly to the algorithm, the expert accuracy also decays when working with small seedlings. However, under these conditions, the expert performance is 10-20% better than the algorithm, although at some points the inter-expert (experts compared to each other) accuracy is not better than the accuracy of the algorithm compared to the experts (Fig. 5). To see if we could improve the accuracy, we trained a new model exclusively on these seedlings and achieved 81% accuracy, 78% precision and 81% recall on the test set. This performance is on par with the experts and points out the importance of the carefully chosen training dataset (Fig S3 and Fig S11). Conclusively, without having solid ground truth data, the training of the algorithm is unavoidably impaired. During the training procedure we annotated about 2500 Arabidopsis hypocotyls, whereas annotating approximately 250 *Sinapis alba* seedlings and about 100 *Brachypodium distachyon* coleoptiles was sufficient to reach similar recognition metric parameters. These data indicate that Arabidopsis is a ‘difficult’ experimental object in terms of hypocotyl measurement, although we must note that our algorithm trained for Arabidopsis is suitable to analyse seedlings with diverse plant architecture, whereas in the case of the two other species we worked with plantlets were grown under only certain conditions.

Future outlook

In recent years, the introduction of deep learning and CNNs revolutionized computer vision-based research, making the automation of various tasks and precise high-throughput

phenotyping available for many disciplines. In plant biology, several advances have been made with these methods regarding qualitative phenotyping (Pound et al., 2017; Namin et al., 2018; Pineda et al., 2018; Singh et al., 2018; Ramcharan et al., 2019). With these tools however, quantitative phenotypic traits can also be assessed as we demonstrated in this work. The presented segmentation pipeline is not only applicable to length measurements, but in principle it can also be used to measure other parameters, such as cotyledon area, hypocotyl hook opening, angle of cotyledons, etc. With the elimination of manual measurements, the current bottleneck in the phenotyping workflow is the ordered laying of the plantlets onto agar plates with special care to avoid overlaps between the plants. This labour-intensive step can be eliminated using object detection frameworks such as Mask-RCNN (He et al., 2017); however, at present these may cause additional segmentation errors, thus reducing accuracy.
While different technical aspects still remain to be overcome, we believe that increasing application and improvement of CNNs for image-based analysis of plants are laying the foundation for the next generation of plant phenotyping tools.

Materials and methods

Code and data availability

The algorithm was implemented in Python, where the PyTorch framework was used for deep learning and the scikit-image library was used for image processing (van der Walt et al., 2014). The code is fully open source and available at GitHub (https://github.com/biomag-lab/hypocotyl-UNet). Images used for training are also available at https://www.kaggle.com/tivadardanka/plant-segmentation. All trained models used in this study are available upon request.

Image acquisition and data preparation

Arabidopsis (*Arabidopsis thaliana*) seedlings were laid manually onto the surface of 1% w/v agar plates. To ensure optimal algorithm performance, the seedlings were arranged without any overlap. During scanning, a black matte cardboard sheet was used as a reflective document mat. The scanning was done using an EPSON PERFECTION V30 scanner at 800 dpi and 24-bit colour setting, and pictures were saved as .tif or .jpg. After the acquisition, hypocotyls, cotyledons, seedcoats and roots were annotated using Fiji (Schindelin et al., 2012). Using the digitizer tablet (WACOM Intuos) instead of a mouse or a touchpad sped up the procedure. The annotated data then were used to create the mask for training the segmentation algorithm. Before training, the images were padded by mirroring a 256 pixel-wide strip next to the border. The padded images were cropped up to non-overlapping pieces with 800x800 pixel resolution, which were used to train the neural network. During training, 10% of the images were held out for validation purposes.
Experts generated data (Expert 1 and Expert 2) by selecting the midline of the hypocotyls with a single piecewise linear curve, from which the length was measured by ImageJ/Fiji.

Training the neural network

To train the U-Net CNN for plant segmentation, about 2500 Arabidopsis hypocotyls, 250 mustard (*Sinapis alba*) seedlings and 100 stiff brome (*Brachypodium distachyon*) plantlets were annotated. For each of the plant species, a different U-Net model was trained. More details on the U-Net architecture can be found in (Ronneberger et al., 2015). As additional regularization, batch normalization layers were used after the convolutional blocks, which was shown to be highly effective for such CNN architectures (Ioffe and Szegedy, 2015). During training, the smooth Dice coefficient loss was used, introduced by (Milletari et al., 2016; Sudre et al., 2017). The model was trained to classify each pixel as (i) background, (ii) hypocotyl (or coleoptile in the case of *Brachypodium distachyon*) or (iii) plant parts not included in the measurement (root, cotyledon, seedcoat, etc.). The output of the UNet model was an RGB image, where every pixel encoded the probability of belonging to one of the three categories (background: red; hypocotyl (or coleoptile): blue; non-hypocotyl plant parts: green). All connected components of the hypocotyl class were skeletonized, followed by pixel counting. No smoothing function was applied. To assure that the plant parts were precisely segmented, their corresponding term in the loss function was weighted fivefold compared to the background. Training was run for 1000 epochs with initial learning rate 1e-4, which was consequently decreased during training to 1e-5, 1e-6 and 1e-7 after epochs 200, 600 and 900. The algorithm was trained using a single nVidia Titan XP GPU. For optimization, the Adam optimizer was used (Kingma and Ba, 2014). To prevent overfitting, batch normalization and image augmentation was used. The augmentation transform was composed as a series of random 512x512 pixel crops, affine transforms with flips and a colour jitter transform. The detailed procedure of reproducing the workflow is described as an instructional help document in the Supplemental Method S1-S2. All presented hypocotyl and coleoptile length data were measured on images which were not involved in the training procedure. We recommend the potential users train the algorithm anew using images depicting plants similar to those to be measured and imaged using the same setup.

Plant growth conditions and light treatments

Arabidopsis (Columbia 0 ecotype) seeds were sown on 4 layers of wet filter paper and were kept at 4 ^{o}C for 3 days. To promote homogeneous germination, plates were exposed to 70-100 µmol m^{-2} s^{-1} white light for 8 h (LUMILUX XT T8 L 36 W/865 fluorescent tubes, Osram), followed by exposure to continuous R (λ_{max}= 660nm), FR (λ_{max}= 735 nm) or B (λ_{max}= 470 nm) light for 4 days at 22 ^{o}C (SNAP-LITE LED light sources, Quantum Devices). Plates containing dark-grown seedlings plates were wrapped in aluminium foil and kept in dark for 4 days at 22^{o}C.
Seeds sown on ½ Murashige and Skoog (MS, Sigma-Aldrich) medium containing 1% w/v sucrose and 0.8% w/v agar were surface sterilised and kept at 4 ^{o}C for 3 days. Seedlings were grown under 12 h white light (80 µmol m^{-2} s^{-1})/ 12 h dark photocycles at 22 ^{o}C in a growth chamber (MLR-350H, SANYO, Gallenkamp) for 7 days. Alternatively, after 3 days, the plates were placed under continuous white light (PHILIPS TL‐ D 18 W/33‐ 640 tubes, 10 μmol m^{-2} s^{-1}) supplemented with UV‐ B (PHILIPS ULTRAVIOLET‐ B TL20W/01RS tubes, 1.5 μmol m^{-2} s^{-1})) for 4 days at 22 °C. The seedlings were covered with transmission cut-off filters (WG series, Schott) using the WG305 filter for UV-B-treated seedlings (+UV-B), and the WG385 filter for the control (-UV-B) seedlings as providing half maximal transmission at 305 or 385 nm, respectively (Bernula et al., 2017).
Brachypodium distachyon (Bd21) seeds were sown on 1% w/v agar and kept at 4 ^{o}C for 5 days and were treated with 24 h white light (130 µmol m^{-2} s^{-1}) to induce even germination. Seedlings were grown either in darkness or under 50 µmol m^{-2} s^{-1} R light or 10 µmol m^{-2} s^{-1} FR light or 130 µmol m^{-2} s^{-1} white light for 4 days. Subsequently, they were placed on a

matte black cardboard sheet and illuminated with even diffused light. Images of the seedlings were taken with a smartphone (iPhone SE, Apple) using the default settings of the camera. Every image contained a millimetre paper for scaling.
Sinapis alba seeds were sown on 1% w/v agar and kept at 4 ^{o}C for 5 days. Seedlings were grown under 130 µmol m^{-2} s^{-1} white light at 22 ^{o}C for 4 days. Seedlings were photographed as described for *Brachypodium distachyon* plants.

Acknowledgments

We thank Dr. János Györgyei for providing the *Brachypodium distachyon* seeds and giving advice on seedling propagation. The work was supported by grants from the Economic Development and Innovation Operative Program (GINOP-2.3.2-15-2016-00001, GINOP-2.3.2-15-2016-00015 and GINOP-2.3.2-15-2016-00026) and from the Hungarian Scientific Research Fund (OTKA, K-132633). T.D. and P.H. acknowledge support from the HAS-LENDULET-BIOMAG and from the European Union and the European Regional Development Fund.

Supplemental Data

Supplemental Figure S1. U-Net segmentation of red light-grown Arabidopsis seedlings.
Supplemental Figure S2. Hypocotyl measurements of Arabidopsis seedlings grown under far-red illumination.
Supplemental Figure S3. U-Net segmentation of far-red light-grown Arabidopsis seedlings.
Supplemental Figure S4. Hypocotyl measurements of Arabidopsis seedlings grown under blue illumination.
Supplemental Figure S5. U-Net segmentation of blue light-grown Arabidopsis seedlings.
Supplemental Figure S6. Hypocotyl measurements of Arabidopsis seedlings grown in the dark or under different white light illumination protocols.
Supplemental Figure S7. Complete U-Net segmentation of Arabidopsis seedlings grown under white light supplied with photomorphogenic UV-B.
Supplemental Figure S8. U-Net segmentation of Sinapis plantlets.
Supplemental Figure S9. U-Net segmentation of Brachypodium plantlets.
Supplemental Figure S10. Student t-test p values for testing effect size between groups.
Supplemental Figure S11. U-Net segmentation of small far-red light-grown Arabidopsis seedlings, using the model trained on small hypocotyls only.
Supplemental Method S1. Creating custom training data.
Supplemental Method S2. Training and using the algorithm.

Figures

Figure 1. Overview of the method.

(a) Arabidopsis seedlings were placed on agar plate surface and scanned, resulting in the original image. This image was then processed by the previously trained U-Net algorithm (see *Materials and Methods* chapter for details), which determines plant parts: hypocotyls (marked with blue colour) and non-hypocotyl plant parts (depicted by green colour). The background pixels appear in red. This step is called segmentation. During the next step, the algorithm determines a 1-pixel-wide line in the middle of the segmented hypocotyls. This procedure is called skeletonization, and the number of pixels consisting of the 1-pixel-wide lines is proportional to the hypocotyl length. White scale bar represents 1 mm.

(b) An example of the graphical representation of the algorithm's output. Besides the quantitative parameters of the detected hypocotyls exported to a *.csv* file, this kind of visualization of the results is also available for the identification of each seedling and for general quality checking of the measurement. The black characters indicate the index of the seedlings in the *.csv* output (N.1., N.2. etc.) whereas the red numbers show the corresponding hypocotyl length in mm.

Figure 2. Hypocotyl measurement of red light-grown Arabidopsis seedlings.

(a) Arabidopsis seedlings were grown on wet filter papers in red light for 4 days, placed on an agar plate and scanned. A close-up image shows a few seedlings grown under high or low fluences of red light and the U-Net segmented and skeletonized images generated from the original by our algorithm. Scale bars represent 1 mm.

(b) This box-and-whisker diagram shows the distribution of seedling hypocotyl length values determined by the algorithm and two human experimenters. Median is marked by a horizontal line inside the box, boxes depict the quartiles, and whiskers extend to show the rest of the distribution. Black diamonds represent outliers. Sample number at every data point is n=30.

Figure 3. *Sinapis alba* hypocotyl and *Brachypodium distachyon* coleoptile measurements by the algorithm.

(a) Original images of light-grown *Sinapis alba* and *Brachypodium distachyon* plantlets (left side). Image panels at the right side depict the segmentation made by the algorithm. The original images also contain a millimetre paper for size scale.

(b) Box-and-whisker diagrams show coleoptile and hypocotyl length values determined by the U-net algorithm and two human experts. Boxes depict the quartiles, whiskers extend to show the rest of the distribution, median is marked by a horizontal line inside the box, whereas black diamonds represent outliers. Sample number for *Sinapis alba* seedlings is n=91 and for *Brachypodium distachyon* plantlets is n≥14 in each light treatment.

Figure 4. Accuracy, recall and precision metrics for the algorithm for each light condition.
Further analysis of the data what are presented in Fig. 2, Fig. 3 and Supplemental Figures S2, S4, S6. Metrics were obtained by matching the plants identified by the algorithm to the ground truth given by the experts. (A match is required to have at least 10% overlap between the bounding boxes of the objects.) *Accuracy* is the relative accuracy of the measurement defined by 1 - |M - L|/L, where L is the ground truth length and M is the measured length. The *precision* of the algorithm is defined as TP/(TP + FP), where TP and FP denote the number of true and false positives, respectively. A high precision implies the majority of identified objects are indeed plants, not false detections. Finally, *recall* is given by TP/(TP + FN), where FN is the number of false negatives. The higher the recall, the more plants were identified by the algorithm.

(a) Analysis of the data obtained on Arabidopsis seedlings. On the left side of the graph, the applied growth conditions are marked: the numbers indicate light intensity in μmol m^{-2} s^{-1}, LD= 12 h light/12 h dark cycles, WL±UVB= white light supplied with or without UV-B, Dark= etiolated seedlings.

(b) The same metrics were calculated from the data obtained on *Brachypodium distachyon* and *Sinapis alba* seedlings.

Figure 5. Intra- and inter-expert accuracies vs the algorithm.
Intra-expert accuracy was calculated by averaging the accuracies between the two measurements from the same expert. *Inter-expert accuracy* (Expert 1 vs Expert 2) was determined by comparing the first measurements of the two human experts. For comparison, the accuracy of the algorithm is also presented.

References

Ádám É, Kircher S, Liu P, Mérai Z, González-Schain N, Hörner M, Viczián A, Monte E, Sharrock RA, Schäfer E, et al (2013) Comparative functional analysis of full-length and N-terminal fragments of phytochrome C, D and E in red light-induced signaling. New Phytol **200**: 86–96

Alves SC, Worland B, Thole V, Snape JW, Bevan MW, Vain P (2009) A protocol for Agrobacterium-mediated transformation of Brachypodium distachyon community standard line Bd21. Nat Protoc **4**: 638–649

Arsovski AA, Galstyan A, Guseman JM, Nemhauser JL (2012) Photomorphogenesis. Arabidopsis Book **10**: e0147

Bernula P, Crocco CD, Arongaus AB, Ulm R, Nagy F, Viczián A (2017) Expression of the UVR8 photoreceptor in different tissues reveals tissue-autonomous features of UV-B signalling: UVR8 signalling in different tissues. Plant Cell Environ **40**: 1104–1114

Borevitz J, Neff M (2008) Phenotypic analysis of Arabidopsis mutants: hypocotyl length. CSH Protoc **2008**: db.prot4962

Buda M, Saha A, Mazurowski MA (2019) Association of genomic subtypes of lower-grade gliomas with shape features automatically extracted by a deep learning algorithm. Comput Biol Med **109**: 218–225

Casal JJ, Qüesta JI (2018) Light and temperature cues: multitasking receptors and transcriptional integrators. New Phytol **217**: 1029–1034

Cole B, Kay SA, Chory J (2011) Automated analysis of hypocotyl growth dynamics during shade avoidance in Arabidopsis. Plant J **65**: 991–1000

Das D, St Onge KR, Voesenek LACJ, Pierik R, Sasidharan R (2016) Ethylene- and Shade-Induced Hypocotyl Elongation Share Transcriptome Patterns and Functional Regulators. Plant Physiol **172**: 718–733

Dieterle M, Thomann A, Renou J-P, Parmentier Y, Cognat V, Lemonnier G, Müller R, Shen W-H, Kretsch T, Genschik P (2005) Molecular and functional characterization of Arabidopsis Cullin 3A. Plant J **41**: 386–399

Fahn A (1990) Plant anatomy. Pergamon

Fankhauser C, Casal JJ (2004) Phenotypic characterization of a photomorphogenic mutant. Plant J **39**: 747–760

Favory J-J, Stec A, Gruber H, Rizzini L, Oravecz A, Funk M, Albert A, Cloix C, Jenkins GI, Oakeley EJ, et al (2009) Interaction of COP1 and UVR8 regulates UV-B-induced photomorphogenesis and stress acclimation in Arabidopsis. EMBO J **28**: 591–601

Geirhos R, Temme CRM, Rauber J, Schütt HH, Bethge M, Wichmann FA (2018) Generalisation in humans and deep neural networks. *In* S Bengio, H Wallach, H Larochelle, K Grauman, N Cesa-Bianchi, R Garnett, eds, Advances in Neural Information Processing Systems 31. Curran Associates, Inc., pp 7549–7561

Gendreau E, Traas J, Desnos T, Grandjean O, Caboche M, Höfte H (1997) Cellular basis of hypocotyl growth in Arabidopsis thaliana. Plant Physiol **114**: 295–305

Hayashi Y, Takahashi K, Inoue S-I, Kinoshita T (2014) Abscisic acid suppresses hypocotyl elongation by dephosphorylating plasma membrane H(+)-ATPase in Arabidopsis thaliana. Plant Cell Physiol **55**: 845–853

He K, Gkioxari G, Dollar P, Girshick R (2017) Mask R-CNN. 2017 IEEE International Conference on Computer Vision (ICCV). IEEE, pp 2980–2988

International Brachypodium Initiative (2010) Genome sequencing and analysis of the model grass Brachypodium distachyon. Nature **463**: 763–768

Ioffe S, Szegedy C (2015) Batch normalization: accelerating deep network training by reducing internal covariate shift. Proceedings of the 32nd International Conference on International Conference on Machine Learning - Volume 37. JMLR.org, pp 448–456

Jung J-H, Domijan M, Klose C, Biswas S, Ezer D, Gao M, Khattak AK, Box MS, Charoensawan V, Cortijo S, et al (2016) Phytochromes function as thermosensors in Arabidopsis. Science **354**: 886–889

Kim BC, Tennessen DJ, Last RL (1998) UV-B-induced photomorphogenesis in Arabidopsis thaliana. Plant J **15**: 667–674

Kingma DP, Ba J (2014) Adam: A Method for Stochastic Optimization. arXiv [cs.LG]

Köhler D (1978) The Course of Ortho-Geotropic Reactions of Shoots. Zeitschrift für Pflanzenphysiologie **87**: 463–467

Lee TC, Kashyap RL, Chu CN (1994) Building Skeleton Models via 3-D Medial Surface Axis Thinning Algorithms. CVGIP: Graphical Models and Image Processing **56**: 462–478

Legris M, Klose C, Burgie ES, Rojas CCR, Neme M, Hiltbrunner A, Wigge PA, Schäfer E, Vierstra RD, Casal JJ (2016) Phytochrome B integrates light and temperature signals in Arabidopsis. Science **354**: 897–900

Lin C, Ahmad M, Cashmore AR (1996) Arabidopsis cryptochrome 1 is a soluble protein mediating blue light-dependent regulation of plant growth and development. Plant J **10**: 893–902

Liscum E, Hangarter RP (1991) Arabidopsis Mutants Lacking Blue Light-Dependent Inhibition of Hypocotyl Elongation. Plant Cell **3**: 685–694

Milletari F, Navab N, Ahmadi S-A (2016) V-Net: Fully Convolutional Neural Networks for Volumetric Medical Image Segmentation. 2016 Fourth International Conference on 3D Vision (3DV). doi: 10.1109/3dv.2016.79

Nagy F, Schäfer E (2002) Phytochromes control photomorphogenesis by differentially regulated, interacting signaling pathways in higher plants. Annu Rev Plant Biol **53**: 329–355

Namin ST, Esmaeilzadeh M, Najafi M, Brown TB, Borevitz JO (2018) Deep phenotyping: deep learning for temporal phenotype/genotype classification. Plant Methods **14**: 66

Pepper AE, Seong-Kim M, Hebst SM, Ivey KN, Kwak SJ, Broyles DE (2001) shl, a New set of Arabidopsis mutants with exaggerated developmental responses to available red, far-red, and blue light. Plant Physiol **127**: 295–304

Pineda M, Pérez-Bueno ML, Barón M (2018) Detection of Bacterial Infection in Melon

Plants by Classification Methods Based on Imaging Data. Front Plant Sci **9**: 164

Pound MP, Atkinson JA, Townsend AJ, Wilson MH, Griffiths M, Jackson AS, Bulat A, Tzimiropoulos G, Wells DM, Murchie EH, et al (2017) Deep machine learning provides state-of-the-art performance in image-based plant phenotyping. GigaScience. doi: 10.1093/gigascience/gix083

Procko C, Crenshaw CM, Ljung K, Noel JP, Chory J (2014) Cotyledon-Generated Auxin Is Required for Shade-Induced Hypocotyl Growth in Brassica rapa. Plant Physiol **165**: 1285–1301

Ramcharan A, McCloskey P, Baranowski K, Mbilinyi N, Mrisho L, Ndalahwa M, Legg J, Hughes DP (2019) A Mobile-Based Deep Learning Model for Cassava Disease Diagnosis. Front Plant Sci **10**: 272

Ronneberger O, Fischer P, Brox T (2015) U-Net: Convolutional Networks for Biomedical Image Segmentation. Medical Image Computing and Computer-Assisted Intervention – MICCAI 2015. Springer International Publishing, pp 234–241

Sangster TA, Salathia N, Undurraga S, Milo R, Schellenberg K, Lindquist S, Queitsch C (2008) HSP90 affects the expression of genetic variation and developmental stability in quantitative traits. Proc Natl Acad Sci U S A **105**: 2963–2968

Schindelin J, Arganda-Carreras I, Frise E, Kaynig V, Longair M, Pietzsch T, Preibisch S, Rueden C, Saalfeld S, Schmid B, et al (2012) Fiji: an open-source platform for biological-image analysis. Nat Methods **9**: 676–682

Scholthof K-BG, Irigoyen S, Catalan P, Mandadi KK (2018) Brachypodium: A Monocot Grass Model Genus for Plant Biology. Plant Cell **30**: 1673–1694

Schopfer P, Oelze-Karow H (1971) [Demonstration of a threshold regulation by phytochrome in the photomodulation of longitudinal growth of the hypocotyl of mustard seedlings (Sinapis alba L.)]. Planta **100**: 167–180

Singh AK, Ganapathysubramanian B, Sarkar S, Singh A (2018) Deep Learning for Plant Stress Phenotyping: Trends and Future Perspectives. Trends Plant Sci **23**: 883–898

Soga K, Yamazaki C, Kamada M, Tanigawa N, Kasahara H, Yano S, Kojo KH, Kutsuna N, Kato T, Hashimoto T, et al (2018) Modification of growth anisotropy and cortical microtubule dynamics in Arabidopsis hypocotyls grown under microgravity conditions in space. Physiol Plant **162**: 135–144

Spalding EP, Miller ND (2013) Image analysis is driving a renaissance in growth measurement. Current Opinion in Plant Biology **16**: 100–104

Sudre CH, Li W, Vercauteren T, Ourselin S, Jorge Cardoso M (2017) Generalised Dice Overlap as a Deep Learning Loss Function for Highly Unbalanced Segmentations. Deep Learning in Medical Image Analysis and Multimodal Learning for Clinical Decision Support 240–248

Vandenbussche F, Verbelen J-P, Van Der Straeten D (2005) Of light and length: regulation of hypocotyl growth in Arabidopsis. Bioessays **27**: 275–284

van der Walt S, Schönberger JL, Nunez-Iglesias J, Boulogne F, Warner JD, Yager N, Gouillart E, Yu T, scikit-image contributors (2014) scikit-image: image processing in Python. PeerJ **2**: e453

Wang L, Uilecan IV, Assadi AH, Kozmik CA, Spalding EP (2009) HYPOTrace: image analysis software for measuring hypocotyl growth and shape demonstrated on Arabidopsis seedlings undergoing photomorphogenesis. Plant Physiol **149**: 1632–1637

Wildermann A, Drumm H, Schäfer E, Mohr H (1978a) Control by light of hypocotyl growth in de-etiolated mustard seedlings : I. Phytochrome as the only photoreceptor pigment. Planta **141**: 211–216

Wildermann A, Drumm H, Schäfer E, Mohr H (1978b) Control by light of hypocotyl growth in de-etiolated mustard seedlings : II. Sensitivity for newly-formed phytochrome after a light to dark transtition. Planta **141**: 217–223

Young JC, Liscum E, Hangarter RP (1992) Spectral-dependence of light-inhibited hypocotyl elongation in photomorphogenic mutants of Arabidopsis: evidence for a UV-A photosensor. Planta **188**: 106–114

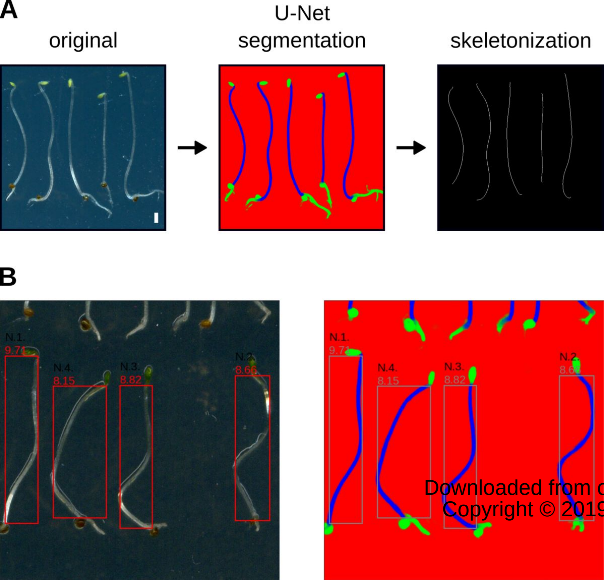
A
original
U-Net segmentation
skeletonization
B
N.1.
9.71
N.4.
8.15
N.3.
8.82
N.2.
8.66

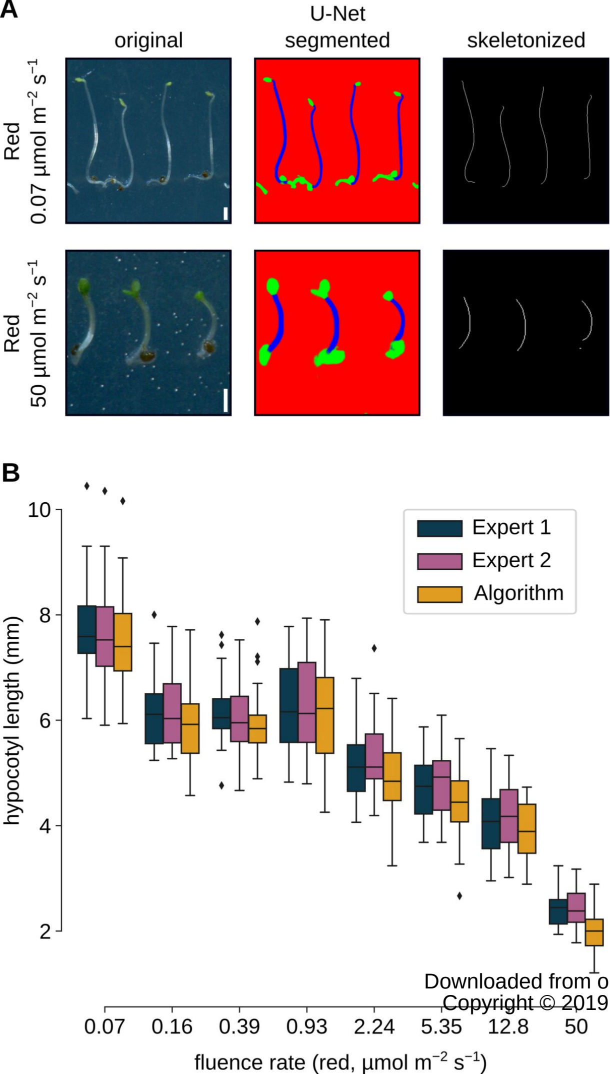

A
original
U-Net segmented
skeletonized
Red 0.07 µmol m⁻² s⁻¹
Red 50 µmol m⁻² s⁻¹
B
hypocotyl length (mm)
Expert 1
Expert 2
Algorithm
0.07
0.16
0.39
0.93
2.24
5.35
12.8
50
fluence rate (red, µmol m⁻² s⁻¹)

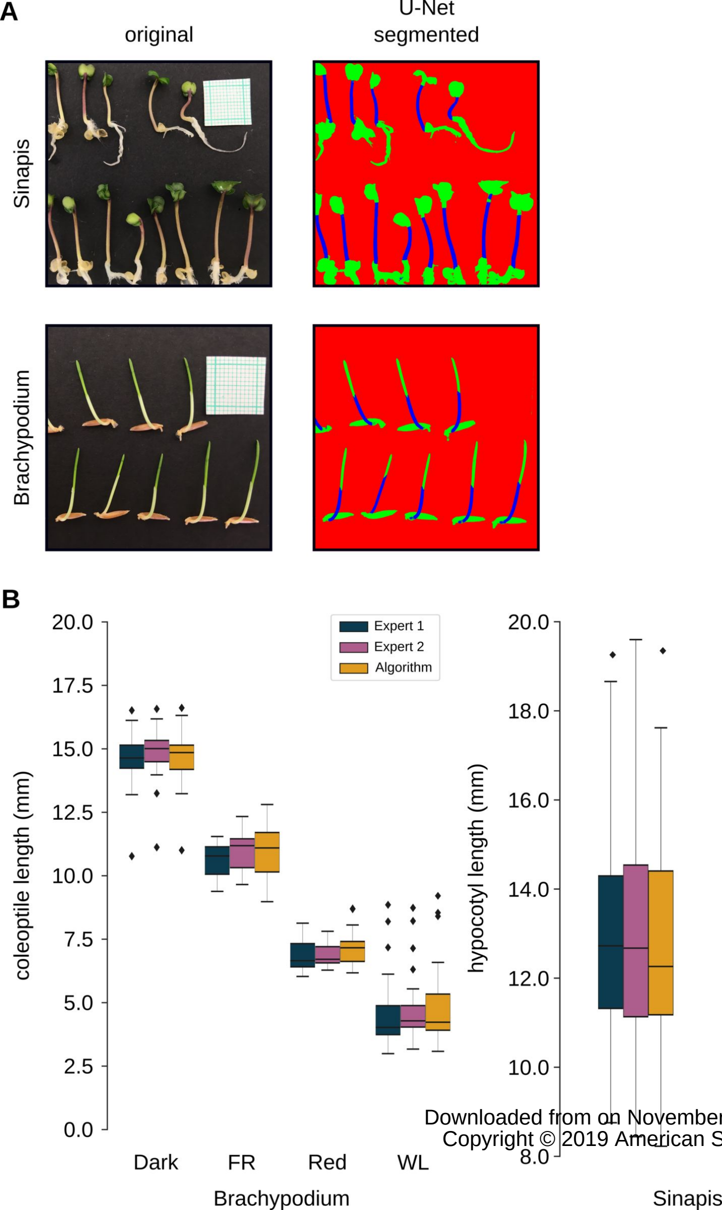
A
original
U-Net
segmented
Sinapis
Brachypodium
B
Expert 1
Expert 2
Algorithm
coleoptile length (mm)
20.0
17.5
15.0
12.5
10.0
7.5
5.0
2.5
0.0
Dark
FR
Red
WL
Brachypodium
hypocotyl length (mm)
20.0
18.0
16.0
14.0
12.0
10.0
8.0
Sinapis

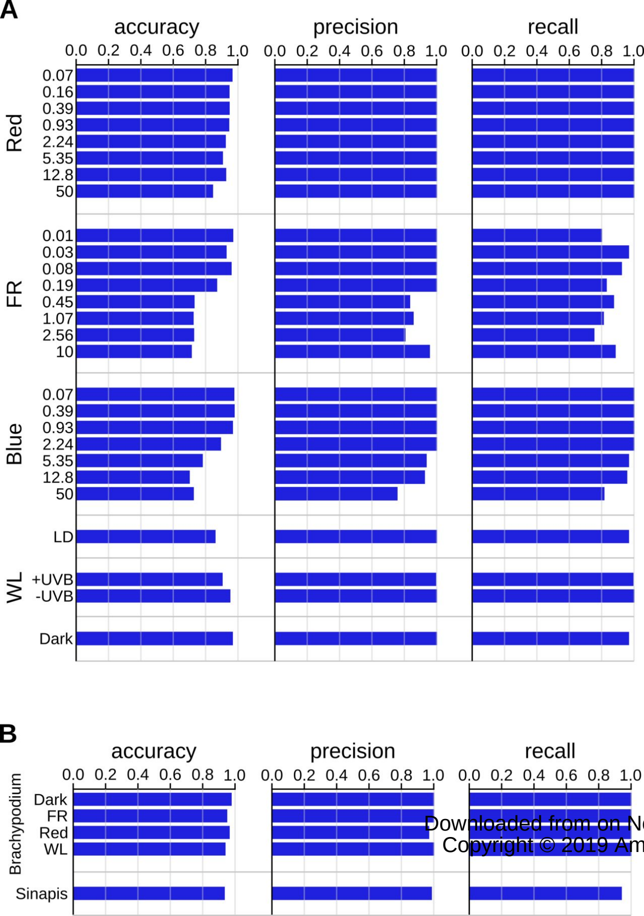
A
accuracy
precision
recall
0.0 0.2 0.4 0.6 0.8 1.0
Red
0.07
0.16
0.39
0.93
2.24
5.35
12.8
50
FR
0.01
0.03
0.08
0.19
0.45
1.07
2.56
10
Blue
0.07
0.39
0.93
2.24
5.35
12.8
50
LD
WL
+UVB
-UVB
Dark
B
Brachypodium
Dark
FR
Red
WL
Sinapis

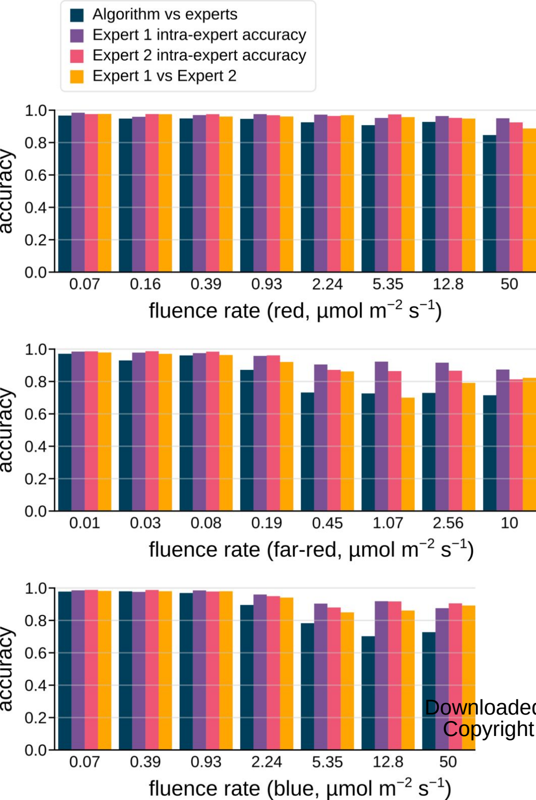
Algorithm vs experts
Expert 1 intra-expert accuracy
Expert 2 intra-expert accuracy
Expert 1 vs Expert 2
accuracy
1.0
0.8
0.6
0.4
0.2
0.0
0.07
0.16
0.39
0.93
2.24
5.35
12.8
50
fluence rate (red, µmol m^{-2} s^{-1})
0.01
0.03
0.08
0.19
0.45
1.07
2.56
10
fluence rate (far-red, µmol m^{-2} s^{-1})
0.07
0.39
0.93
2.24
5.35
12.8
50
fluence rate (blue, µmol m^{-2} s^{-1})

Parsed Citations

Ádám É, Kircher S, Liu P, Mérai Z, González-Schain N, Hörner M, Viczián A, Monte E, Sharrock RA, Schäfer E, et al (2013) Comparative functional analysis of full-length and N-terminal fragments of phytochrome C, D and E in red light-induced signaling. New Phytol 200: 86–96
Pubmed: Author and Title
Google Scholar: Author Only Title Only Author and Title

Alves SC, Worland B, Thole V, Snape JW, Bevan MW, Vain P (2009) A protocol for Agrobacterium-mediated transformation of Brachypodium distachyon community standard line Bd21. Nat Protoc 4: 638–649
Pubmed: Author and Title
Google Scholar: Author Only Title Only Author and Title

Arsovski AA, Galstyan A, Guseman JM, Nemhauser JL (2012) Photomorphogenesis. Arabidopsis Book 10: e0147
Pubmed: Author and Title
Google Scholar: Author Only Title Only Author and Title

Bernula P, Crocco CD, Arongaus AB, Ulm R, Nagy F, Viczián A (2017) Expression of the UVR8 photoreceptor in different tissues reveals tissue-autonomous features of UV-B signalling: UVR8 signalling in different tissues. Plant Cell Environ 40: 1104–1114
Pubmed: Author and Title
Google Scholar: Author Only Title Only Author and Title

Borevitz J, Neff M (2008) Phenotypic analysis of Arabidopsis mutants: hypocotyl length. CSH Protoc 2008: db.prot4962
Pubmed: Author and Title
Google Scholar: Author Only Title Only Author and Title

Buda M, Saha A, Mazurowski MA (2019) Association of genomic subtypes of lower-grade gliomas with shape features automatically extracted by a deep learning algorithm. Comput Biol Med 109: 218–225
Pubmed: Author and Title
Google Scholar: Author Only Title Only Author and Title

Casal JJ, Qüesta JI (2018) Light and temperature cues: multitasking receptors and transcriptional integrators. New Phytol 217: 1029–1034
Pubmed: Author and Title
Google Scholar: Author Only Title Only Author and Title

Cole B, Kay SA, Chory J (2011) Automated analysis of hypocotyl growth dynamics during shade avoidance in Arabidopsis. Plant J 65: 991–1000
Pubmed: Author and Title
Google Scholar: Author Only Title Only Author and Title

Das D, St Onge KR, Voesenek LACJ, Pierik R, Sasidharan R (2016) Ethylene- and Shade-Induced Hypocotyl Elongation Share Transcriptome Patterns and Functional Regulators. Plant Physiol 172: 718–733
Pubmed: Author and Title
Google Scholar: Author Only Title Only Author and Title

Dieterle M, Thomann A, Renou J-P, Parmentier Y, Cognat V, Lemonnier G, Müller R, Shen W-H, Kretsch T, Genschik P (2005) Molecular and functional characterization of Arabidopsis Cullin 3A. Plant J 41: 386–399
Pubmed: Author and Title
Google Scholar: Author Only Title Only Author and Title

Fahn A (1990) Plant anatomy. Pergamon
Pubmed: Author and Title
Google Scholar: Author Only Title Only Author and Title

Fankhauser C, Casal JJ (2004) Phenotypic characterization of a photomorphogenic mutant. Plant J 39: 747–760
Pubmed: Author and Title
Google Scholar: Author Only Title Only Author and Title

Favory J-J, Stec A, Gruber H, Rizzini L, Oravecz A, Funk M, Albert A, Cloix C, Jenkins GI, Oakeley EJ, et al (2009) Interaction of COP1 and UVR8 regulates UV-B-induced photomorphogenesis and stress acclimation in Arabidopsis. EMBO J 28: 591–601
Pubmed: Author and Title
Google Scholar: Author Only Title Only Author and Title

Geirhos R, Temme CRM, Rauber J, Schütt HH, Bethge M, Wichmann FA (2018) Generalisation in humans and deep neural networks. In S Bengio, H Wallach, H Larochelle, K Grauman, N Cesa-Bianchi, R Garnett, eds, Advances in Neural Information Processing Systems 31. Curran Associates, Inc., pp 7549–7561
Pubmed: Author and Title
Google Scholar: Author Only Title Only Author and Title

Gendreau E, Traas J, Desnos T, Grandjean O, Caboche M, Höfte H (1997) Cellular basis of hypocotyl growth in Arabidopsis

thaliana. Plant Physiol 114: 295–305
Pubmed: Author and Title
Google Scholar: Author Only Title Only Author and Title

Hayashi Y, Takahashi K, Inoue S-I, Kinoshita T (2014) Abscisic acid suppresses hypocotyl elongation by dephosphorylating plasma membrane H(+)-ATPase in Arabidopsis thaliana. Plant Cell Physiol 55: 845–853
Pubmed: Author and Title
Google Scholar: Author Only Title Only Author and Title

He K, Gkioxari G, Dollar P, Girshick R (2017) Mask R-CNN. 2017 IEEE International Conference on Computer Vision (ICCV). IEEE, pp 2980–2988
Pubmed: Author and Title
Google Scholar: Author Only Title Only Author and Title

International Brachypodium Initiative (2010) Genome sequencing and analysis of the model grass Brachypodium distachyon. Nature 463: 763–768
Pubmed: Author and Title
Google Scholar: Author Only Title Only Author and Title

Ioffe S, Szegedy C (2015) Batch normalization: accelerating deep network training by reducing internal covariate shift. Proceedings of the 32nd International Conference on International Conference on Machine Learning - Volume 37. JMLR.org, pp 448–456
Pubmed: Author and Title
Google Scholar: Author Only Title Only Author and Title

Jung J-H, Domijan M, Klose C, Biswas S, Ezer D, Gao M, Khattak AK, Box MS, Charoensawan V, Cortijo S, et al (2016) Phytochromes function as thermosensors in Arabidopsis. Science 354: 886–889
Pubmed: Author and Title
Google Scholar: Author Only Title Only Author and Title

Kim BC, Tennessen DJ, Last RL (1998) UV-B-induced photomorphogenesis in Arabidopsis thaliana. Plant J 15: 667–674
Pubmed: Author and Title
Google Scholar: Author Only Title Only Author and Title

Kingma DP, Ba J (2014) Adam: A Method for Stochastic Optimization. arXiv [cs.LG]
Pubmed: Author and Title
Google Scholar: Author Only Title Only Author and Title

Köhler D (1978) The Course of Ortho-Geotropic Reactions of Shoots. Zeitschrift für Pflanzenphysiologie 87: 463–467
Pubmed: Author and Title
Google Scholar: Author Only Title Only Author and Title

Lee TC, Kashyap RL, Chu CN (1994) Building Skeleton Models via 3-D Medial Surface Axis Thinning Algorithms. CVGIP: Graphical Models and Image Processing 56: 462–478
Pubmed: Author and Title
Google Scholar: Author Only Title Only Author and Title

Legris M, Klose C, Burgie ES, Rojas CCR, Neme M, Hiltbrunner A, Wigge PA, Schäfer E, Vierstra RD, Casal JJ (2016) Phytochrome B integrates light and temperature signals in Arabidopsis. Science 354: 897–900
Pubmed: Author and Title
Google Scholar: Author Only Title Only Author and Title

Lin C, Ahmad M, Cashmore AR (1996) Arabidopsis cryptochrome 1 is a soluble protein mediating blue light-dependent regulation of plant growth and development. Plant J 10: 893–902
Pubmed: Author and Title
Google Scholar: Author Only Title Only Author and Title

Liscum E, Hangarter RP (1991) Arabidopsis Mutants Lacking Blue Light-Dependent Inhibition of Hypocotyl Elongation. Plant Cell 3: 685–694
Pubmed: Author and Title
Google Scholar: Author Only Title Only Author and Title

Milletari F, Navab N, Ahmadi S-A (2016) V-Net: Fully Convolutional Neural Networks for Volumetric Medical Image Segmentation. 2016 Fourth International Conference on 3D Vision (3DV). doi: 10.1109/3dv.2016.79
Pubmed: Author and Title
Google Scholar: Author Only Title Only Author and Title

Nagy F, Schäfer E (2002) Phytochromes control photomorphogenesis by differentially regulated, interacting signaling pathways in higher plants. Annu Rev Plant Biol 53: 329–355
Pubmed: Author and Title
Google Scholar: Author Only Title Only Author and Title

Namin ST, Esmaeilzadeh M, Najafi M, Brown TB, Borevitz JO (2018) Deep phenotyping: deep learning for temporal phenotype/genotype classification. Plant Methods 14: 66
Pubmed: Author and Title
Google Scholar: Author Only Title Only Author and Title

Pepper AE, Seong-Kim M, Hebst SM, Ivey KN, Kwak SJ, Broyles DE (2001) shl, a New set of Arabidopsis mutants with exaggerated developmental responses to available red, far-red, and blue light. Plant Physiol 127: 295–304
Pubmed: Author and Title
Google Scholar: Author Only Title Only Author and Title

Pineda M, Pérez-Bueno ML, Barón M (2018) Detection of Bacterial Infection in Melon Plants by Classification Methods Based on Imaging Data. Front Plant Sci 9: 164
Pubmed: Author and Title
Google Scholar: Author Only Title Only Author and Title

Pound MP, Atkinson JA, Townsend AJ, Wilson MH, Griffiths M, Jackson AS, Bulat A, Tzimiropoulos G, Wells DM, Murchie EH, et al (2017) Deep machine learning provides state-of-the-art performance in image-based plant phenotyping. GigaScience. doi: 10.1093/gigascience/gix083
Pubmed: Author and Title
Google Scholar: Author Only Title Only Author and Title

Procko C, Crenshaw CM, Ljung K, Noel JP, Chory J (2014) Cotyledon-Generated Auxin Is Required for Shade-Induced Hypocotyl Growth in Brassica rapa. Plant Physiol 165: 1285–1301
Pubmed: Author and Title
Google Scholar: Author Only Title Only Author and Title

Ramcharan A, McCloskey P, Baranowski K, Mbilinyi N, Mrisho L, Ndalahwa M, Legg J, Hughes DP (2019) A Mobile-Based Deep Learning Model for Cassava Disease Diagnosis. Front Plant Sci 10: 272
Pubmed: Author and Title
Google Scholar: Author Only Title Only Author and Title

Ronneberger O, Fischer P, Brox T (2015) U-Net: Convolutional Networks for Biomedical Image Segmentation. Medical Image Computing and Computer-Assisted Intervention – MICCAI 2015. Springer International Publishing, pp 234–241
Pubmed: Author and Title
Google Scholar: Author Only Title Only Author and Title

Sangster TA, Salathia N, Undurraga S, Milo R, Schellenberg K, Lindquist S, Queitsch C (2008) HSP90 affects the expression of genetic variation and developmental stability in quantitative traits. Proc Natl Acad Sci U S A 105: 2963–2968
Pubmed: Author and Title
Google Scholar: Author Only Title Only Author and Title

Schindelin J, Arganda-Carreras I, Frise E, Kaynig V, Longair M, Pietzsch T, Preibisch S, Rueden C, Saalfeld S, Schmid B, et al (2012) Fiji: an open-source platform for biological-image analysis. Nat Methods 9: 676–682
Pubmed: Author and Title
Google Scholar: Author Only Title Only Author and Title

Scholthof K-BG, Irigoyen S, Catalan P, Mandadi KK (2018) Brachypodium: A Monocot Grass Model Genus for Plant Biology. Plant Cell 30: 1673–1694
Pubmed: Author and Title
Google Scholar: Author Only Title Only Author and Title

Schopfer P, Oelze-Karow H (1971) [Demonstration of a threshold regulation by phytochrome in the photomodulation of longitudinal growth of the hypocotyl of mustard seedlings (Sinapis alba L.)]. Planta 100: 167–180
Pubmed: Author and Title
Google Scholar: Author Only Title Only Author and Title

Singh AK, Ganapathysubramanian B, Sarkar S, Singh A (2018) Deep Learning for Plant Stress Phenotyping: Trends and Future Perspectives. Trends Plant Sci 23: 883–898
Pubmed: Author and Title
Google Scholar: Author Only Title Only Author and Title

Soga K, Yamazaki C, Kamada M, Tanigawa N, Kasahara H, Yano S, Kojo KH, Kutsuna N, Kato T, Hashimoto T, et al (2018) Modification of growth anisotropy and cortical microtubule dynamics in Arabidopsis hypocotyls grown under microgravity conditions in space. Physiol Plant 162: 135–144
Pubmed: Author and Title
Google Scholar: Author Only Title Only Author and Title

Spalding EP, Miller ND (2013) Image analysis is driving a renaissance in growth measurement. Current Opinion in Plant Biology 16: 100–104
Pubmed: Author and Title
Google Scholar: Author Only Title Only Author and Title

Sudre CH, Li W, Vercauteren T, Ourselin S, Jorge Cardoso M (2017) Generalised Dice Overlap as a Deep Learning Loss Function for Highly Unbalanced Segmentations. Deep Learning in Medical Image Analysis and Multimodal Learning for Clinical Decision Support 240–248
Pubmed: Author and Title
Google Scholar: Author Only Title Only Author and Title

Vandenbussche F, Verbelen J-P, Van Der Straeten D (2005) Of light and length: regulation of hypocotyl growth in Arabidopsis. Bioessays 27: 275–284
Pubmed: Author and Title
Google Scholar: Author Only Title Only Author and Title

van der Walt S, Schönberger JL, Nunez-Iglesias J, Boulogne F, Warner JD, Yager N, Gouillart E, Yu T, scikit-image contributors (2014) scikit-image: image processing in Python. PeerJ 2: e453
Pubmed: Author and Title
Google Scholar: Author Only Title Only Author and Title

Wang L, Uilecan IV, Assadi AH, Kozmik CA, Spalding EP (2009) HYPOTrace: image analysis software for measuring hypocotyl growth and shape demonstrated on Arabidopsis seedlings undergoing photomorphogenesis. Plant Physiol 149: 1632–1637
Pubmed: Author and Title
Google Scholar: Author Only Title Only Author and Title

Wildermann A, Drumm H, Schäfer E, Mohr H (1978a) Control by light of hypocotyl growth in de-etiolated mustard seedlings : I. Phytochrome as the only photoreceptor pigment. Planta 141: 211–216
Pubmed: Author and Title
Google Scholar: Author Only Title Only Author and Title

Wildermann A, Drumm H, Schäfer E, Mohr H (1978b) Control by light of hypocotyl growth in de-etiolated mustard seedlings : II. Sensitivity for newly-formed phytochrome after a light to dark transtition. Planta 141: 217–223
Pubmed: Author and Title
Google Scholar: Author Only Title Only Author and Title

Young JC, Liscum E, Hangarter RP (1992) Spectral-dependence of light-inhibited hypocotyl elongation in photomorphogenic mutants of Arabidopsis: evidence for a UV-A photosensor. Planta 188: 106–114
Pubmed: Author and Title
Google Scholar: Author Only Title Only Author and Title